Earth Planet. Sci. Lett. 674 (2026) 119740

Contents lists available at ScienceDirect

Earth and Planetary Science Letters

journal homepage: www.elsevier.com/locate/epsl

Fractionated nickel isotopic compositions in the subducting slab – implications for mantle heterogeneity

Naomi J. Saunders [a,1,*], Baptiste Debret [b], Jason Harvey [c], Edward Inglis [d], Alex N. Halliday [a,e]

[a] Lamont-Doherty Earth Observatory, Columbia University, 61 Route 9W, Palisades 10964, USA
[b] Institut de physique du globe de Paris, Université Paris Cité, CNRS, Paris, France
[c] School of Earth and Environment, University of Leeds, Leeds LS2 9JT, UK
[d] School of Earth and Environmental Science, Cardiff University, Park Place, Cardiff CF10 3AT, UK
[e] Dept of Earth Sciences, University of Oxford, South Parks Road, Oxford OX1 3AN, UK

ARTICLE INFO

Edited by\Dr Fang-Zhen Teng

Keywords:
Stable isotopes
Nickel
Metamorphism
Serpentinites
Mantle recycling

ABSTRACT

It has been hypothesized that Ni isotope heterogeneities in ultramafic xenoliths, mid-ocean ridge basalts (MORB) and ocean island basalts (OIB) might originate from recycled components. Eclogitic and blueschist facies ultramafic, basaltic, and gabbroic lithologies from the SW Alps have Ni isotopic compositions ($\delta^{60/58}$Ni) extending from -0.5 to +0.3 ‰, overlapping well with the values found in oceanic basalts and mantle xenoliths. The Queyras blueschist facies metagabbros display the lightest Ni isotope compositions (-0.5 to +0.2 ‰), correlating negatively with enrichment in fluid mobile elements such as Li and Sb, consistent with isotopic fractionation during metasomatism. The Zermatt eclogites and Allalin gabbros define a more restricted range of $\delta^{60/58}$Ni, with metabasalts (-0.2 to +0.1 ‰) lighter than metagabbros (+0.1 to +0.3 ‰); the latter overlapping with published results for typical un-metasomatized lherzolites and harzburgites. Eclogitic serpentinites from Monvisoare similar ($\delta^{60/58}$Ni = 0.0 to +0.3 ‰). Only metasediments are isotopically heavy ($\delta^{60/58}$Ni = +0.1 to +0.7 ‰), except for one greenschist facies metagabbro from Chenaillet (+0.7 ‰). Published data for seafloor alteration of oceanic crust do not explain the variations. Indeed, abyssal serpentinites from the Atlantic Ocean, included for comparison as a putative Ni-rich recycled protolith, display highly variable $\delta^{60/58}$Ni (+0.3 to +1.2 ‰), heavier than any reported MORB, OIB or ultramafic xenoliths, and with an apparent hyperbolic relation with $^{187}Os/^{188}Os$, possibly reflecting ancient sulfide removal or some form of alteration process in antiquity. Subduction of high pressure metamorphic mafic assemblages like those of the SW Alps provide an enriched source component with light $\delta^{60/58}$Ni that could contribute to the Ni isotope heterogeneity found in MORB, OIB, and peridotite and pyroxenite xenoliths.

1. Introduction

The Earth's mantle contains 97 % of the nickel in the silicate Earth (McDonough and Sun, 1995), reflecting the similarity in charge and ionic radius of Ni and Mg, hence strong compatibility of Ni during melting. Nickel isotopic compositions do not fractionate significantly during mantle melting (Klaver et al., 2024; Saunders et al., 2020). Despite this, plus the overwhelming budgetary dominance of the mantle, Ni stable isotope data for unaltered basalts and peridotite xenoliths define a range of values that far exceed the limits of analytical uncertainty ($\delta^{60/58}$Ni = −0.19 ‰ to +0.36 ‰; Klaver et al., 2020; Saunders et al., 2022, Saunders et al., 2020; Wang et al., 2021; Yang et al., 2023) with lighter $\delta^{60/58}$Ni associated with indicators of incompatible element and Fe enrichment (Klaver et al., 2020; Saunders et al., 2020, 2022). Even lighter $\delta^{60/58}$Ni is found in some pyroxenites, extending to −0.38 ‰ (Saunders et al., 2020).

Some pyroxenites are thought to represent recycled basaltic oceanic crust (e.g. Zhang et al., 2019). Therefore, to explore whether this unexpected mantle heterogeneity is caused by recycling of ocean floor materials we have studied relict slab sections (meta-ophiolites) from the Western Alps that preserve evidence for blueschist and eclogite facies conditions, and that were metamorphosed and obducted during the Alpine orogeny. These Alpine meta-ophiolites record well-defined prograde metamorphic conditions that are taken to be representative of a

* Corresponding author.
E-mail address: naomi.saunders@mail.com (N.J. Saunders).
[1] Present address: Department of Earth Sciences, Royal Holloway University of London, Egham, Surrey, UK, TW20 0EX

https://doi.org/10.1016/j.epsl.2025.119740
Received 17 January 2025; Received in revised form 12 November 2025; Accepted 13 November 2025
Available online 22 November 2025

P-T path for subducting mafic oceanic crust and exhibit varying degrees of slab metasomatism, from fluids derived from proximal subducting sediments (Inglis et al., 2017). Such features, combined with extensive literature data, e.g. Dale et al. (2007, 2009), Debret et al. (2016a) and Inglis et al. (2017), make this sample set ideal for studying how such large-scale metamorphism could fractionate the Ni isotope compositions of subducted materials. We compare the Ni isotope composition of high pressure and temperature (HP-HT) lithologies to pre-existing datasets for altered oceanic crust (Gall, 2011; Gueguen et al., 2013) and new data on serpentinized Ni-rich abyssal peridotites from the 15° 20N Fracture Zone area on the Mid-Atlantic Ridge. The behaviour of Ni in subduction zones is not well understood, so these results provide insights into the processes that cause elemental Ni redistribution and isotope fractionation relevant to the sources of arc volcanism.

2. Geological setting and sample descriptions

2.1. Subducted ocean floor

The Western Alps are a natural laboratory for studying fluid-mediated transfer during subduction (Scambelluri and Philippot, 2001). Alpine meta-ophiolites were metamorphosed at typical subduction zone P-T conditions, and preserve their prograde metamorphic history (Agard, 2021). These meta-ophiolites are mainly composed of serpentinites enveloping metagabbros. They were highly hydrated and serpentinized during an oceanic stage in a distal continental margin or mid-ocean ridge environment, prior to partial dehydration during prograde metamorphism (Agard, 2021). We selected twenty high-pressure rocks from four localities across the Western Alps, namely the Chenaillet ophiolite, the Queyras Schiste Lustrés complex, and the Monviso and Zermatt Zaas meta-ophiolites. These record various P-T conditions, from greenschist to eclogite facies, and simulate a subduction P-T gradient (see Supplementary Figure 1 for location and P-T record). An extended geological background is provided in the Supplementary Information (SI 1.1)

The Chenaillet Massif is an obducted ophiolite forming a klippe sitting structurally on the Queyras Schiste Lustrés nappes, 6 km west of Briançon (France). It mainly preserves low-pressure ocean floor parageneses that range from amphibolite to greenschist facies P-T conditions (e.g. Debret et al., 2016b). The sample analysed (PR4) here is an undeformed, coarse grained gabbro comprising mainly plagioclase, clinopyroxene and brown amphibole with minor (<10 %) actinolite (Inglis et al., 2017).

The Queyras Schistes Lustrés complex consists of 10 % meta-ophiolites and 90 % of metasedimentary rocks strongly deformed during alpine subduction. It is thought to be derived from a sedimentary wedge (Tricart and Schwartz, 2006). The complex can be divided in three tectono-metamorphic units recording increasing P-T conditions from east (0.9 to 1.1 GPa and 320–370 °C) to west (2 GPa and 400–470 °C; e.g. Schwartz et al., 2013). The Queyras meta-ophiolites are considered to represent an open system where fluids released during meta-sediment dehydration infiltrated the surrounding rocks during subduction, resulting in extensive HP-HT fluid-rock interaction between different lithologies (e.g. Debret et al., 2016a). For this study, we selected six blueschist metagabbros (QE10, BB1, RV7, CE12, TR6, TR9) and one blueschist metasediment (RV5). The Queyras metagabbros are mainly composed of magmatic clinopyroxene relics, low-pressure amphibole (e.g., hornblende, actinolite), ilmenite, titanite, glaucophane, lawsonite and chlorite with variable amounts of albite, epidote, and quartz. Textural relationships show that glaucophane and lawsonite (± epidote, quartz) replaced low pressure amphibole and plagioclase assemblages with increasing P-T conditions from west to east (Debret et al., 2016b). The Queyras metasediments are mainly made of paragonite, phengite, chlorite, carpholite, lawsonite, chloritoid, glaucophane, and quartz.

The Monviso meta-ophiolite is an eclogitic mafic/ultramafic unit extending over 30 km along strike at the French–Italian border (Supplementary Figure 1). There are limited metasedimentary rocks observed at this locality (<10 %). It is separated from the blueschist-facies Queyras Schistes Lustrés Complex to the west by a ductile normal fault. Despite its length, the Monviso Massif largely preserves the structure of the oceanic lithosphere with homogeneous P-T conditions of 520–570 °C and 2.6–2.7 GPa for the entire meta-ophiolite (Caurant et al., 2023). We selected two meta-serpentinites (Vis1F, Vis5b) and two metasediments (Vis 18–13, Vis 18–17) for this study. The Monviso meta-serpentinites are formed by the eclogite facies olivine, antigorite, ± titanoclinohumite paragenesis resulting from brucite breakdown at HP-HT (Schwartz et al., 2013). The Monviso metasedimentary rocks typically display the eclogite-facies kyanite-jadeite-garnet paragenesis (Herviou et al., 2023).

The Zermatt Zaas complex is located further north, in Switzerland. It represents continuous oceanic slices with ultramafic, mafic, and metasedimentary lithologies metamorphosed at eclogite facies conditions. Metagabbro and metabasalt samples from the Allalin gabbroic body (S01/5G, S02/83viiiG, S01/35iix) and the Mattmark moraine (S01/40viix, S02/85ixE, S01/40vx, and S02/85ixB) were selected for this study (Inglis et al., 2017). Samples S01/5G and S02/83viiixG are fresh gabbro preserving a primary gabbroic mineral assemblage with no evidence of HP-HT overprint ('ocean-like' in figures hereafter). Eclogitic samples (S01/35iix, S01/40viix, S02/85ixE, S01/40vx) display classic eclogite assemblages of garnet, omphacite, paragonite, glaucophane, and phengite while sample S02/85ixB displays evidence of retrograde metamorphism. The metamorphic climax of the Allalin gabbro (S01/5G, S02/83viiiG, S01/35iix) and the Mattmark moraine (S01/40viix, S02/85ixE, S01/40vx, and S02/85ixB), is 2.5 GPa and 610 °C, which contrasts with Zermatt Saas Pfulwe location at ~0.25 GPa and 550–600 °C (Inglis et al., 2017).

2.2. Abyssal serpentinites

The abyssal serpentinites are from two drill cores in the 15° 20N Fracture Zone area on the Mid-Atlantic Ridge collected during ODP Leg 209 (See Supplementary Figure 2). In general, harzburgites from Hole 1274A are fresher than 1268A, and 1274A dunites are more highly serpentinized than harzburgites from the same core (Kelemen et al., 2004a). A more extensive geological background is provided in the Supplementary Information (SI 1.2).

The 1268A ultramafic lithologies exhibit an unusual continuous decrease in orthopyroxene between harzburgite and dunite, rather than the more usual bimodal distribution (Kelemen et al., 2004b). Osmium isotopes provide evidence that the melting that formed the residual harzburgites at Hole 1274A occurred up to 2 Gyr ago followed by decompression related melt extraction and percolation under the modern MOR (Harvey et al., 2006). In Hole 1268A, samples have been affected by pervasive serpentinization and overprinting by pervasive talc alteration (steatitization) under static conditions (Bach et al., 2004). Bach et al. (2004) suggest that the talc alteration in Hole 1268A is due to silica metasomatism mobilized during high-temperature (>350 °C) fluid-rock interactions in harzburgites and gabbros. Klein and Bach (2009) proposed a maximum temperature of 300 °C for the serpentinization at Hole 1268A and 200 °C in 1274A based on bimodal Co distribution in pentlandites. Sulfides are only present in veins in Hole 1274A up to 0.4 % modal percent, compared to abundant sulfides in Hole 1268A (Kelemen et al., 2004b).

We have analysed 3 samples from Hole 1268A of which two are talc-altered serpentinites and the third a serpentinized harzburgite. Of the 6 samples from Hole 1274A, 4 are serpentinized harzburgites and 2 serpentinized dunites.

3. Analytical methods

Analytical work was carried out in the Department of Earth Sciences,

University of Oxford and in the Novel Isotopes in Climate, Environment, and Rocks (NICER) laboratories of Lamont-Doherty Earth Observatory (LDEO), Columbia University. Nickel purification was carried out in a metal-free clean laboratory using the three-stage ion exchange chemistry described in Saunders et al. (2022, 2020), based on Gall et al. (2012), using PTFE heat shrink micro-columns of diminishing size (615 µl, 250 µl, and 120 µl).

Nickel isotope compositions were determined by measuring ^{58}Ni, ^{60}Ni, ^{61}Ni, and ^{62}Ni in pseudo-high resolution on either a Nu Plasma HR MC-ICPMS (Oxford), or a Nu Plasma Sapphire MC-ICPMS in High Energy mode (LDEO), with each Faraday collector using a 10^{-11} Ω resistor. The analysed masses were measured on the low mass peak shoulder in order to avoid variable polyatomic interferences, especially on mass 58. Mass 57 was monitored for correction of the isobaric interference of ^{58}Fe on ^{58}Ni. A statistical rejection removed data that was outside acceptable range (2 standard error) from the online calculations. To further reduce the effect of any residual uncorrected polyatomic interferences or matrix effects, samples and standards were intensity matched to give a total Ni signal of ~15 V (Oxford) to ~35–55 V (LDEO). Data reduction for the deconvolution of the double spike was performed online followed by offline normalisation to the bracketing standard NIST SRM986. Nickel concentrations were calculated by isotope dilution from the fractionation-corrected double spiked Ni isotopic composition.

The accuracy and precision of our methods were assessed by repeated analysis of USGS reference materials and in house Fe-Ni sulfides in each analytical session. At least one USGS reference material (BHVO2, BIR1a, PCC1, or DTS2) was processed with each sample batch and analysed over more than one session. Based on the above analyses of rock reference materials the within-laboratory reproducibility, equivalent to external reproducibility of this study was assessed as ±0.06 ‰ (2 σ). This was equal to the maximum 2 standard deviations from the repeated replicates of USGS rock standards. This uncertainty is used for all representative error bars in the figures in this paper. Extended information on methods, including values obtained for the analysis of reference materials and standard solutions, is provided in the Supplementary Information (SI 2).

4. Results

Nickel concentrations and isotopic compositions are presented in Tables 1 and 2 and compared with published data for a variety of potentially relevant lithologies and reservoirs in Fig. 1. The studied samples cover a wide range in Ni concentrations from 53 to 3070 µg.g^{-1}, with highest concentrations, as expected, in the serpentinites. Nickel concentrations in metabasalts are lower on average than an average for their protoliths, whereas for metagabbros there is no significant difference. The 3 metabasalts average 68 ± 17 µg.g^{-1} (2SE) compared with a MORB average of 98 ± 2 µg.g^{-1} (2SE, n = 2679) (Gale et al., 2013). The 14 metagabbro samples average 188 ± 66 µg.g^{-1} (2SE), comparable to the gabbro average in Godard et al. (2009) of 158 µg.g^{-1}. The four olivine metagabbros (metagabbros with Mg#>0.8, (Inglis et al., 2017)) average 323 ± 73 µg.g^{-1} (2SE), comparable with the published olivine gabbro average of 305 ± 40 µg.g^{-1} (2SE, n = 72) (Godard et al., 2009). The 10 metagabbros with Mg# between 0.7 and 0.8 average 118 ± 30 µg.g^{-1} (2SE). Given the variability within pristine gabbros and basalts, these data do not indicate Ni loss. There is no significant difference in Ni concentration between the abyssal serpentinites (1649 to 2170 µg.g^{-1}) and some mantle estimates, e.g., 1860 µg.g^{-1} (Palme and O'Neill, 2007).

The $\delta^{60/58}$Ni for the Alpine meta-ophiolite samples in this study also span a wide range from −0.50 ± 0.02 ‰ to +0.76 ± 0.08 ‰. Distinct lithologies and locations display very different isotopic compositions, even for specific sub-types (e.g. those samples that had basaltic or gabbroic protoliths).

The average $\delta^{60/58}$Ni for the metamorphic samples in this study is +0.13 ± 0.60 ‰ (2SD, n = 20), and basaltic / gabbroic types average $\delta^{60/58}$Ni = +0.07 ± 0.58 ‰ (2SD, n = 15). When combined with the literature eclogite data of Wang et al. (2021) the meta-igneous average is $\delta^{60/58}$Ni = +0.06 ± 0.48 ‰ (2SD, n = 22). Metasediments from this study preserve the largest range in Ni isotope compositions ($\delta^{60/58}$Ni = +0.09 ‰ to +0.76 ‰, n = 3), consistent with the wide range of published marine sediment data (−0.79 ‰ to +2.50 ‰, average $\delta^{60/58}$Ni = +0.50 ± 1.15 ‰, n = 137, 2SD; Ciscato et al., 2018; Fleischmann et al., 2023; Little et al., 2020; Pašava et al., 2019; Porter et al., 2014). Eclogite facies samples are heavier in $\delta^{60/58}$Ni than blueschist facies samples of the same protolith lithology. Specifically, eclogite metagabbros average $\delta^{60/58}$Ni = +0.21 ± 0.16 ‰ (n = 7, 2SD) whereas blueschist

Table 1
Metamorphosed samples with Ni isotope data, Ni concentration by isotope dilution, and n = number of replicate analyses with 2SD on those replicates.

Sample	Lithology	Facies	General location	Ni conc by ID (µg.g^{-1})	$\delta^{60/58}$Ni (‰)	2SD	n
Vis 18–13	metasediment	eclogite	Monviso	75.1	+0.759	0.075	3
Vis 18–17	metasediment	eclogite	Monviso	57.5	+0.357	0.053	2
Vis1F	serpentinite	eclogite	Monviso	3070	+0.042	0.051	5
Vis5b	serpentinite	eclogite	Monviso	1566	+0.286	0.052	9
RV5	metasediment	blueschist	Queyras	55.9	+0.085	0.015	3
QE10	metagabbro	blueschist	Queyras	226.7	−0.040	0.023	3
BB1	metagabbro	blueschist	Queyras	88.3	−0.371	0.047	4
RV7	metagabbro	blueschist	Queyras	134.7	+0.008	0.076	5
CE12	metagabbro	blueschist	Queyras	87.4	−0.483	0.029	5
TR6	metagabbro	blueschist	Queyras	67.9	+0.192	0.040	3
TR9	metagabbro	blueschist	Queyras	67.0	−0.013	0.024	3
S01/40viix	metagabbro (olivine)	eclogite	Zermatt, Mattmark	343.3	+0.292	0.042	3
S02/85ixE	metagabbro	eclogite	Zermatt, Mattmark	133.8	+0.240	0.060	3
S02/85ixB	metagabbro	eclogite, with evidence of late retrogression	Zermatt, Mattmark	165.3	+0.147	0.032	3
S01/40vx	metagabbro (olivine)	eclogite	Zermatt, Mattmark	286.5	+0.182	0.043	3
S02/75iiR	metabasalt	eclogite	Zermatt, Pfulwe	63.3	+0.058	0.027	2
S02/75iiiR	metabasalt	eclogite	Zermatt, Pfulwe	87.2	−0.175	0.021	3
S02/41v	metabasalt	eclogite	Zermatt, Pfulwe	52.8	−0.105	0.055	3
S01/35iiix	metagabbro	eclogite	Zermatt, Allalin	121.6	+0.325	0.031	2
S01/5G	metagabbro (olivine)	ocean-like	Zermatt, Allalin	483.3	+0.165	0.019	4
S02/83viiixG	metagabbro (olivine)	ocean-like	Zermatt, Allalin	338.0	+0.080	0.052	4
PR4	metagabbro	greenschist / ocean-like	Chenaillet	86.4	+0.749	0.043	7

Table 2
Abyssal serpentinite data with Ni isotope data, Ni concentration by isotope dilution, and n = number of replicate analyses with 2SD on those replicates.

Hole	Core	Lith	Grid reference	Depth in core (cm)	Metres below sea floor (mbsf)	Ni conc by ID (μg.g^{-1})	$\delta^{60/58}$Ni (‰)	2SD	n
1268A	8R1	serpentinite (talc-altered)	14°50 N 45°25′W	28–35	44.28	1688	+0.460	0.074	4
1268A	16R2	serpentinite (talc-altered)	14°50 N 45°25′W	88–94	84.49	1650	+0.427	0.016	3
1268A	2R2	serpentinized harzburgite	14°50 N 45°25′W	27–35	15.19	1664	+0.497	0.072	2
1274A	4R1	serpentinized harzburgite	15°38 N 46°40′W	30–36	21.6	1938	+1.177	0.089	3
1274A	7R1	serpentinized harzburgite	15°38 N 46°40′W	68–74	36.48	1715	+0.402	0.022	2
1274A	12R2	serpentinized harzburgite	15°38 N 46°40′W	35–41	59.75	1905	+0.397	0.036	3
1274A	17R2	serpentinized harzburgite	15°38 N 46°40′W	27–33	88.57	1703	+0.394	0.051	2
1274A	8R1	serpentinized dunite	15°38 N 46°40′W	72–88	40.72	2171	+0.278	0.024	3
1274A	25R1	serpentinized dunite	15°38 N 46°40′W	63–69	137.13	1716	+0.918	0.053	2

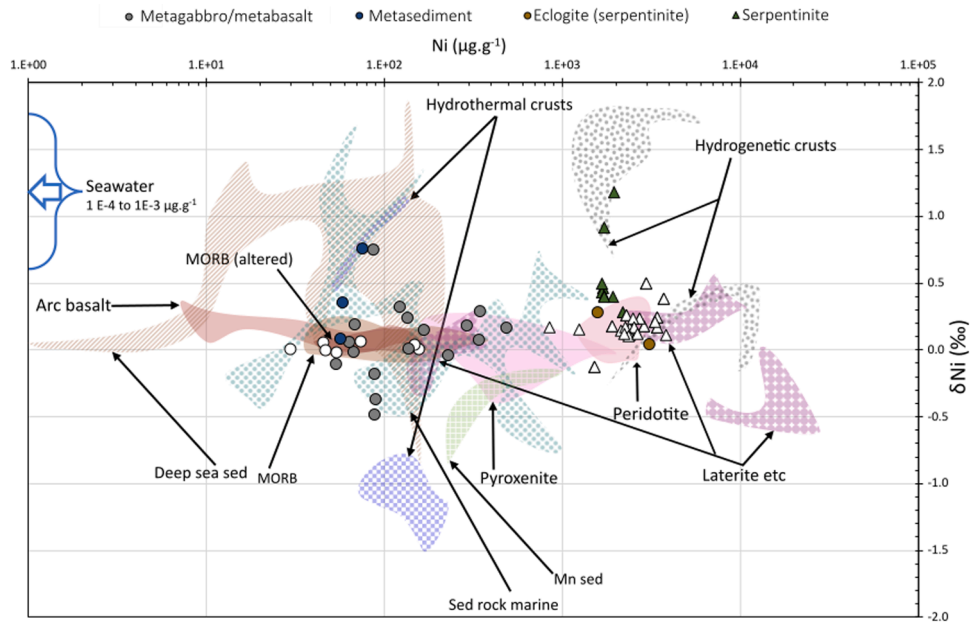

Fig. 1. Nickel isotopic compositions for the data presented in this paper (solid symbols) relative to literature equivalents (open symbols) Serpentinites references (Dong et al., 2024; Gall, 2011; Gueguen et al., 2013; Machado et al., 2023; Spivak-Birndorf et al., 2018; Wang et al., 2021). Also shown: solid zones for other high temperature lithologies (Gall, 2011; Gall et al., 2017; Gueguen et al., 2013; Klaver et al., 2020; Ratié et al., 2015; Saunders et al., 2022, Saunders et al., 2020; Wang et al., 2021; Yang et al., 2023), and patterned zones for other seafloor related and altered lithologies relative to the above (Ciscato et al., 2018; Fleischmann et al., 2023; Gall, 2011; Gueguen et al., 2021, Gueguen et al., 2013; Gueguen and Rouxel, 2021; He et al., 2023; Little et al., 2020; Machado et al., 2023; Pašava et al., 2019; Porter et al., 2014; Ratié et al., 2016, 2015; Spivak-Birndorf et al., 2018; Sun et al., 2024). Seawater references (e.g. Archer et al., 2020; Cameron and Vance, 2014; Lemaitre et al., 2022; Takano et al., 2022, 2017; Wang et al., 2019). Eoarchean peridotites and intraplate igneous materials are not shown.

metagabbros average $\delta^{60/58}$Ni = −0.12 ± 0.47 ‰ (n = 6, 2SD); and eclogite facies metasediments average $\delta^{60/58}$Ni = +0.56 ± 0.40 ‰ (n = 2, 2SD), whereas the single blueschist facies metasediment has $\delta^{60/58}$Ni of +0.09 ‰ (n = 1). Excluding the two metagabbros with preserved primary mineral assemblages (S01/5G and S02/83viiixG) barely changes the average eclogitic metagabbro $\delta^{60/58}$Ni to +0.24 ± 0.13 ‰ (n = 5, 2SD). Eclogitic metabasalts (average $\delta^{60/58}$Ni = −0.07 ± 0.20 ‰, n = 3, 2SD), are between eclogitic metagabbros and blueschist metagabbros in Ni isotopic composition. The two eclogitic serpentinites give results of $\delta^{60/58}$Ni = +0.04 ± 0.05 ‰ (5 replicate analyses) and +0.29 ± 0.05 ‰ (9 replicate analyses), also between eclogitic metagabbros and blueschist metagabbros in Ni isotopic composition. The average $\delta^{60/58}$Ni for Zermatt metagabbros with Mg# ≤ 0.8 (+0.24 ± 0.11 ‰, 2SD, n = 2) and Mg# > 0.8 (+0.24 ± 0.15 ‰, 2SD, n = 3) are identical. Average unmetasomatised mantle peridotite (+0.14 ± 0.11 ‰; 2SD, n = 44; Klaver et al. 2020; Saunders et al., 2020; Wang et al., 2021) falls between these two samples. The single greenschist-facies meagabbro from this study contrasts starkly with other high-temperature samples from both this study and from the literature, with a $\delta^{60/58}$Ni of +0.74 ± 0.04 ‰ (2SD on 7 individual analyses). This locality is not associated with Alpine metamorphism, the greenschists reflecting a later overprint (Inglis et al., 2017). However, it provides evidence that high- and low-pressure metamorphic processes and fluids have influenced the Ni isotopic compositions very differently.

From the blueschist Queyras locality, two metagabbros from medium temperature (340–360 °C) and four from high temperature (380–470 °C) domains were sampled. The medium temperature samples (CE12 = −0.48 ‰, QE10 = −0.04 ‰), define a smaller range than the high

temperature domain samples (BB1 = −0.37 ‰, TR9 = −0.0 1 ‰, RV7 = +0.01 ‰, TR6 = +0.19 ‰). The high temperature metasediment sample falls within the high temperature metagabbro range (RV5 = +0.09 ‰).

Of the Zermatt Saas samples, two gabbros with primary mineral assemblages ('ocean-like', Allalin) have $\delta^{60/58}$Ni of +0.17 ‰ (S01/5G) and +0.08 ‰ (S02/83viiixG). Of the remaining metagabbros the sample with the lightest $\delta^{60/58}$Ni (+0.15 ‰) has evidence of late retrogression (S02/85ixB), whereas the sample with the heaviest $\delta^{60/58}$Ni is also from Allalin (S01/35iiix = +0.33 ‰). Of the metabasalts from Zermatt Saas, two are from the rim of the same pillow basalt (S02/75iiR = +0.06 ‰ and S02/75iiiR = −0.18 ‰), whereas the last is from a massive basalt (S01/41v = −0.11 ‰).

At the Monviso locality, as with the samples from Queyras, the metasediments have the heaviest $\delta^{60/58}$Ni determined (Vis18–17 = +0.36 ‰, Vis18–13 = +0.76 ‰), whereas two eclogite-facies serpentinites with mantle protoliths are lighter (Vis1F = +0.04 ‰, Vis5b = +0.29 ‰).

Of the abyssal serpentinites, the overall range in $\delta^{60/58}$Ni is consistently heavy (+0.28 ‰ to +1.18 ‰) compared to previously reported data for samples of basaltic ocean floor material (−0.22 ‰ to +0.19 ‰, (Gall, 2011; Saunders et al., 2022; Wang et al., 2021). Harzburgitic serpentinites range in $\delta^{60/58}$Ni between +0.39 ‰ and +1.18 ‰ (average = +0.57 ± 0.61 ‰,) and dunitic serpentinites range from +0.28 ‰ to +0.92 ‰ (average +0.60 ± 0.64 ‰). Samples from Hole 1268A average +0.46 ± 0.06 ‰ (n = 3), with no resolvable difference from those of Hole 1274A (+0.59 ± 0.66 ‰ (n = 6)). Two samples from 1268A are talc altered but their average composition of +0.44 ± 0.03 ‰, is within uncertainty, identical to that of non-talc altered serpentinized samples, which average +0.58 ± 0.61 ‰. All these abyssal serpentinites have strikingly heavy Ni isotopic compositions compared with any ultramafic xenoliths yet reported (Gall et al., 2017; Klaver et al., 2020; Ratié et al., 2015; Saunders et al., 2020; Wang et al., 2021) (Fig. 1).

5. Discussion: the causes of Ni isotopic fractionation

5.1. Nickel isotopes in abyssal serpentinites and ancient silicate-sulfide fractionation

The Ni isotopic compositions of the abyssal serpentinites are highly variable, extending to values that are heavier (+0.28 ‰ to +1.18 ‰) than anything previously reported for mantle-derived materials. These samples are variably serpentinized and so an obvious first question is whether this reflects interaction with isotopically heavy Ni from seawater (weighted average $\delta^{60/58}$Ni = +1.37 ‰: Archer et al., 2020; Cameron and Vance, 2014; Lemaitre et al., 2022; Little et al., 2020; Takano et al., 2022, 2017; Wang et al., 2019)). This seems unlikely because the Hole 1274A harzburgites are less serpentinized than the associated dunites (Kelemen et al., 2004a), yet the $\delta^{60/58}$Ni is similar. Furthermore, the concentration of Ni in seawater is so low (averaging 2.93 × 10^{-4} μg.g^{-1} Archer et al., 2020; Cameron and Vance, 2014; Lemaitre et al., 2022; Takano et al., 2022; Wang et al., 2019) that altering the Ni isotopic compositions from normal mantle to such heavy values would require water / rock ratios of the order of 10^6. Additionally, there is no significant Ni loss in this sample suite compared to average pristine protolith concentrations. Therefore, seawater alteration is, at first sight, an unlikely mechanism for producing heavy $\delta^{60/58}$Ni in abyssal serpentinites. Nonetheless, major variations in $\delta^{60/58}$Ni, including heavy values, have been recorded in heavily weathered serpentinites (Machado et al. 2023).

A second possible explanation is that variations in $\delta^{60/58}$Ni are affected by sulfide alteration. Nickel concentration is not correlated with S abundance in abyssal peridotites from these cores (Supplementary Figure 3) regardless of the absence or presence of talc alteration. This seems to rule out late-stage sulfide mineralisation as an agent of Ni isotope fractionation. For the three samples with S data in our $\delta^{60/58}$Ni dataset, no significant relationship is observed. Sulphur in unserpentinized mantle is usually restricted to 200 ± 50 μg.g^{-1} (Palme and O'Neill, 2007). Sulfide as a discrete phase is present at <0.03 modal %, of which pentlandite, the only primary mantle sulfide that carries a significant wt. % of Ni, is only a small fraction. Sulphur contents in the abyssal serpentinites of this study (n = 3) are highly variable from "normal" mantle values up to 0.55 wt. % (Paulick et al., 2006). Talc alteration in Hole 1268A samples is associated with a marked increase in S abundance. Sulfide mineralization differs in its nature by locality, with the S from Hole 1268A being hosted primarily in veins and up to 3 wt. % in bulk material (Miller, 2007), whereas veins in 1274A have a maximum of 0.4 % sulfide (Kelemen et al., 2004a) and substantially lower S concentrations overall. Both sites exhibit evidence of heavy Ni isotope compositions, but no association is seen between heavier $\delta^{60/58}$Ni and more extreme S abundances attributable to the hydrothermal fluids associated with talc formation (Paulick et al., 2006). In recent work on intraplate basalts, Dong et al. (2024) used Cu to monitor sulfide involvement in mantle melting on $\delta^{60/58}$Ni – a relationship which is not observed in this work (Supplementary Figure 4).

A clue to the possible cause of the heavy $\delta^{60/58}$Ni in abyssal peridotite samples lies in the Os isotopic compositions. In fact, this is the *only* parameter that shows a systematic relationship with $\delta^{60/58}$Ni. Six of the samples studied, all from Hole 1274A, have associated Os isotopic data (Harvey et al. 2006), which define an apparent hyperbolic trend between the mass dependent $\delta^{60/58}$Ni fractionation and radiogenic $^{187}Os/^{188}Os$, with the heaviest $\delta^{60/58}$Ni associated with unradiogenic Os, and vice versa (Fig. 5). This relationship is the opposite of that expected from seawater alteration. The $^{187}Os/^{188}Os$ of present-day seawater is about 1 (e.g. Gannoun and Burton, 2014) so cannot explain the heavy $\delta^{60/58}$Ni endmember, which is associated with ancient, mantle-like unradiogenic $^{187}Os/^{188}Os$ of 0.118. Seawater $^{187}Os/^{188}Os$ has changed over time and was as low as 0.4 in the Paleocene (Ravizza et al., 2001). The Os isotopic composition of seawater prior to this is not well constrained but is expected to include a major component of radiogenic Os from continental erosion. Conversely, an $^{187}Os/^{188}Os$ of 0.118, associated with heavy $\delta^{60/58}$Ni is exactly what is to be expected as the time-integrated effect of low $^{187}Re/^{188}Os$, predicted for strongly depleted mantle. The relationship with Os isotope composition also precludes a diffusion process for the observed Ni isotopes fractionation, as there would be no cause for diffusion to affect both isotope systems in this way, given that Os is corrected for isotopic fractionation.

One possible explanation is that these heavy Ni isotope compositions predate seafloor alteration, and that the oceanic crust and upper mantle contain ancient, strongly depleted peridotites, with unusually heavy $\delta^{60/58}$Ni. The apparent hyperbolic trend in Fig. 5 is too strongly curved to reflect simple mixing. This would require an orders of magnitude difference in [Os] between the two end members, whereas the measured serpentinite concentrations vary by only a factor of 5 (Harvey et al. 2006). There also is no known mechanism for achieving this trend via silicate-melt fractionation (Klaver et al., 2024, Klaver et al., 2020; Saunders et al., 2020). However, sulfides often carry isotopically light $\delta^{60/58}$Ni (Gueguen et al., 2013; Hofmann et al., 2014; Pašava et al., 2019; Smith et al., 2022) as well as fractionated *Re*/Os (e.g. (Dale et al., 2007)). Ancient equilibrium fractionation with a sulfide liquid with high *Re*/Os and light $\delta^{60/58}$Ni, could potentially leave a silicate residue, with variable *Re*/Os and isotopically fractionated Ni. There are no functional relationships discernible between [Ni] and either Ni isotopic composition, or $^{187}Os/^{188}Os$. However, the $^{187}Os/^{188}Os$ does show a broad trend with $^{187}Re/^{188}Os$ that might relate to fractionation at around 1 Ga (Harvey et al. 2006). Therefore, the present Ni concentrations presumably reflect in part more recent unrelated disturbances, such as from extensive seawater alteration.

Such heavy $\delta^{60/58}$Ni is unusual in mantle-derived samples (Gall et al., 2017; Saunders et al., 2022; Wang et al., 2021; Yang et al., 2023). However, similarly heavy $\delta^{60/58}$Ni, ranging from +0.07 ‰ to +1.00 ‰, has been identified in Siberian Trap basalts (Chen et al., 2023). These

have also been ascribed to enrichment in heavy $\delta^{60/58}$Ni in residual silicate melt following sulfide segregation. There is a strong negative relationship between heavy $\delta^{60/58}$Ni and Ni content in the Siberian Trap samples (Chen et al., 2023), which would be consistent with recent redistribution of chalcophile elements in the abyssal peridotites. However, no such relationship is observed in this new dataset.

Alteration of Ni-rich rocks in a tropical continental weathering environment can display highly variable Ni isotopic compositions ranging from −0.57 ‰ to +0.52 ‰, where more negative $\delta^{60/58}$Ni compositions are observed closer to the surface of the weathering profile (R^2 = 0.73, data from Machado et al., 2023). These samples show a moderate inverse covariation between $\delta^{60/58}$Ni and Ni concentrations (R^2 = 0.52, data from Machado et al., 2023), unlike that observed in the serpentinites of this work. The ultramafic parent serpentinite has $\delta^{60/58}$Ni = +0.24 ‰ and +0.26 ‰ (Machado et al., 2023), both examples being lighter than the lightest $\delta^{60/58}$Ni observed in our serpentinite dataset.

Recently, it has been shown that most arcs display Mg isotopic compositions that are heavier than those of normal mantle-derived rocks (Fan et al., 2024; Yuan et al., 2023). Fan et al. (2024) relate the mobility of Mg in subduction zones to the presence of serpentinite, with some dependence on the temperature of the arc system. Nickel isotopic compositions would provide a powerful test of this interpretation of the Mg isotope data. The only Ni isotope data currently available on arc basalts are from Kamchatka, a cold arc that shows average Mg isotopic compositions that are identical to those of the mantle (Fan et al., 2024). These data on evolved magmas are not comparable to the dataset presented here, and the relationships observed in Kamchatka are not observed within our dataset. For Ni this is also true with an average $\delta^{60/58}$Ni of +0.11 ‰ (n = 19). However, the data do range to unusually heavy compositions of +0.34 ‰ (Yang et al., 2023), which might reflect a serpentinite component.

5.2. *The Ni isotopic variations in the metamorphic assemblages are not inherited from the protolith oceanic crust*

Given that the metamorphic samples studied here are of oceanic lithospheric origin, it is worth evaluating whether any of the Ni isotopic variations might be inherited from such a protolith. Nickel isotope compositions of fresh and altered MORB have been published previously (Gall, 2011; Gueguen et al., 2013; Saunders et al., 2022; Wang et al., 2021), and with abyssal serpentinites also investigated in this work, a wider range of possible subduction zone input compositions can now be evaluated.

Altered MORB studied thus far exhibits a range of $\delta^{60/58}$Ni from −0.03 to +0.14 ‰, with an average of +0.05 ± 0.11 ‰ (2SD; n = 11) (Gall, 2011; Gueguen et al., 2013), which is entirely within the extremes of pristine MORB samples (−0.22 to +0.19 ‰; average of +0.02 ± 0.20 ‰, n = 30, 2SD; Gall, 2011; Saunders et al., 2022; Wang et al., 2021). Both altered and pristine sample sets yield the same average $\delta^{60/58}$Ni of +0.05 ‰, when arithmetically weighted by Ni concentration. Therefore, seafloor alteration of the oceanic crust does not appear a likely cause of the Ni isotope variability in the mantle-derived samples studied so far. There is no overlap in $\delta^{60/58}$Ni between meta-igneous samples studied here and MORB datasets (Fig. 1). The relationships between chemical parameters such as La/Yb (Fig. 2), which can be controlled by magmatic differentiation, and $\delta^{60/58}$Ni in meta-igneous samples are also unlike those found in MORB.

Any Ni isotope fractionation stemming from magmatic differentiation would be expected to generate a covariation with [Ni] (Fig. 4) or [Mg] (Supplementary Figure 5), such as observed in Yang et al. (2023), which is not observed in this dataset. Furthermore, the work by Klaver et al. (2024) showed that silicate mineral Ni isotope fractionation is negligible except for that observed between clinopyroxene and olivine. Further, experiments showed that olivine-melt equilibrium could only produce a small fractionation +0.004 to −0.047 ‰ (Klaver et al., 2024).

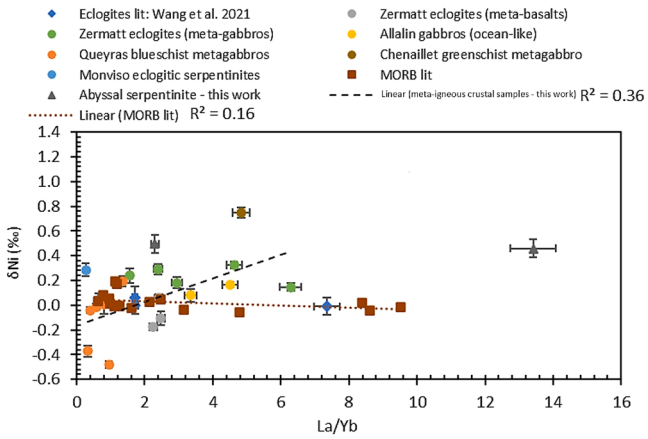

Fig. 2. Contrasting relationships observed in La/Yb with MORB dataset (Saunders et al., 2022; Wang et al., 2021) and new Alpine metamorphosed data. Error bars on Ni isotope composition are 2SD on repeated analyses of the sample. X axis error bars of 5 % equivalent to worst case scenario.

This magnitude of fractionation cannot reproduce the range of values observed in this dataset. Further, the Ni concentrations relate directly to Mg# (calculated by total moles Mg / total moles Mg + total moles Fe, as in (Inglis et al., 2017) in the expected way. Yet there is no relationship is observed between $\delta^{60/58}$Ni and Mg# across a range of values.

Nickel isotopic variations in subduction zones could also be introduced by subducted ferromanganese deposits such as metalliferous sediments, hydrogenetic crusts, hydrothermal crusts and Mn nodules. Light $\delta^{60/58}$Ni compositions have been recorded in hydrothermal Fe-Mn oxide deposits, which are actively forming low temperature hydrothermal deposits associated with microbial mats (Gueguen et al., 2021). Similarly, Mn-rich sediments from marginal locations in the Pacific show isotopically light $\delta^{60/58}$Ni compositions (Fleischmann et al., 2023; Little et al., 2020). However, some deep ocean manganese-rich pelagic sediments (Fleischmann et al., 2023) provide evidence of a variably Ni-rich component with heavy $\delta^{60/58}$Ni that could also contribute to the budget of subducted Ni. Ferromanganese crusts and nodules (Gall et al., 2013; Gueguen et al., 2021) have extremely heavy $\delta^{60/58}$Ni (+0.33 ‰ to +2.47 ‰), as well as being very Ni-rich (1162 to 11,850 μg.g^{-1}). A comparatively small input of Ni from these isotopically distinct sources has the potential to shift the $\delta^{60/58}$Ni of subducted metabasalt rocks to higher values. The $\delta^{60/58}$Ni of the metabasaltic and metagabbroic samples of this study (putting aside the one greenschist facies sample) range only up to the heaviest values found in N-MORB and less enriched peridotites. There is therefore no evidence for mass transfer from isotopically much heavier Ni-rich ferromanganese crusts. Nickel concentrations do not correlate with $\delta^{60/58}$Ni. Therefore, it seems more likely that the Ni isotopes are fractionated during exchange with metamorphic fluids rather than by mixing with a high Ni concentration reservoir.

5.3. *Evidence of fluid mobility and isotopic fractionation of Ni in subduction environments*

Isotopes of fluid mobile elements can be fractionated, either by kinetic or equilibrium processes and this has been demonstrated for Ni at low temperatures as a result of weathering (e.g. Gall, 2011; Machado et al., 2023; Ratié et al., 2015; Spivak-Birndorf et al., 2018; Sun et al., 2024; Wu et al., 2022). In general, such fluid–rock interaction leaves an altered mineral assemblage with light $\delta^{60/58}$Ni. As discussed above, variable Ni isotopic compositions have been observed in Ni-rich rocks altered in continental weathering – including values as light as −0.57 ‰ between 3 – 7 m of a 45 m profile analysed of an Amazonian weathering profile of an exposed mafic-ultramafic intrusive complex (Machado

et al., 2023). To what extent major Ni isotope fractionation also occurs at higher temperatures is less clear, although magmatic processes have been shown to have little effect. Metasomatic fluids associated with the formation of nephelinites derived by high fO_2 melting have been hypothesised to have light $\delta^{60/58}$Ni, although, sulfide may also have played a role (Sheng et al., 2022). Hydrothermal fluids have been implicated in the production of heavy $\delta^{60/58}$Ni in native metals produced during interactions between fresh lava and seawater (Hawco et al., 2020). The high-pressure metamorphic environment studied here though is very different and is largely unexplored with respect to Ni isotope systematics.

Of the samples derived from gabbroic protoliths, the eclogite-facies metagabbro samples have a $\delta^{60/58}$Ni range of +0.08 ‰ to +0.33 ‰, averaging +0.21 ± 0.16 ‰ (2SD, $n = 7$) whereas the blueschist-facies metagabbros are significantly lighter, with a range of −0.48 ‰ to +0.19 ‰, and averaging −0.12 ± 0.47 ‰ (2SD; $n = 6$). This difference between rocks that have identical protoliths but have experienced different pressure and temperature conditions in contrasting regions of a subduction zone, provides powerful evidence that metamorphic fluids are responsible for modifying $\delta^{60/58}$Ni during subduction. The one sample with clear retrograde effects (S02/85ixB) does not show a fractionated isotopic signature (+0.15 ± 0.03 ‰). It is comparable with the isotopic composition of the Bulk Silicate Earth and the average of the entire sample set.

This contrasts with the highly fractionated results found across the pristine prograde blueschist metagabbro sequence. These rocks display striking negative correlations (Fig. 3) between Ni isotopic composition

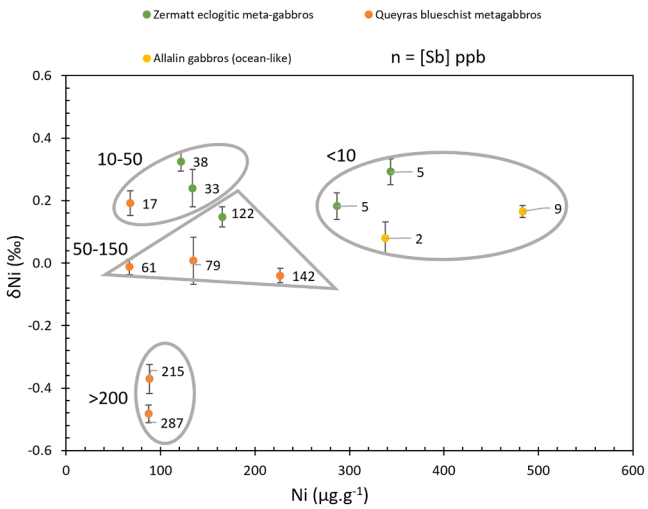

Fig. 4. Nickel concentration and Ni isotopic composition for Alpine sample set contoured for Sb content. Error bars on Ni isotope composition are 2SD on repeated analyses of the sample. Ni concentration analysed by isotope dilution; error bars contained within symbols.

and the concentrations of various fluid mobile elements. For example, [Li] is strongly correlated (R^2=0.83) as is Li/Y (R^2=0.76), a parameter that is elevated in arc lavas (Elliott et al., 2004). The lightest $\delta^{60/58}$Ni

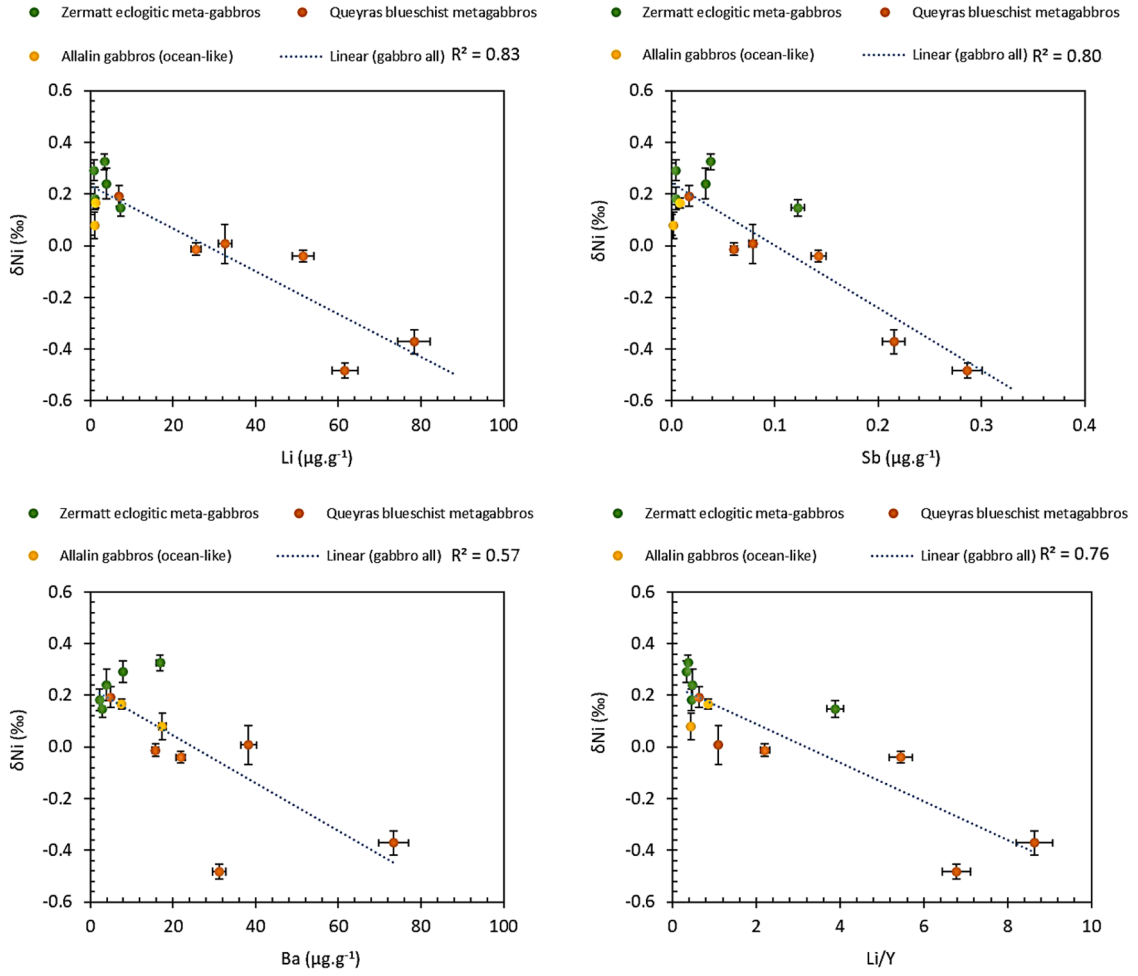

Fig. 3. Observed relationships in new meta-gabbro dataset for light Ni isotopic compositions associated with higher concentrations in certain fluid mobile elements. Error bars on Ni isotope composition are 2SD on repeated analyses of the sample. X axis error bars a worst case 5 %.

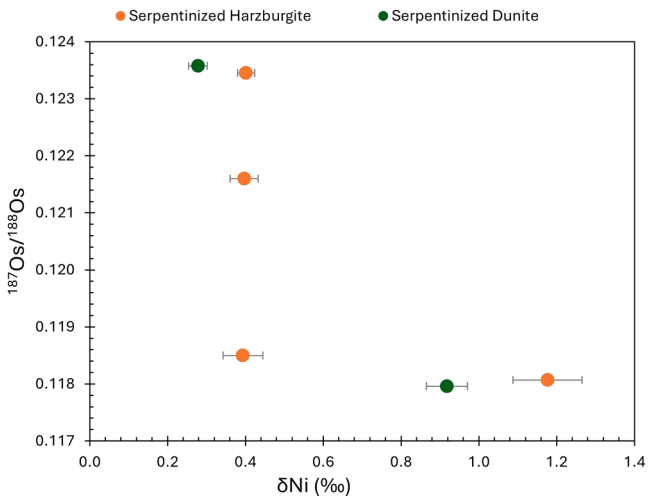

Fig. 5. Figure showing the asymptotic mixing relationship between Os isotopic composition and Ni isotopic composition. Osmium isotope data from (Harvey et al., 2006). Error bars on Ni isotope composition are 2SD on repeated analyses of the sample.

and highest Li concentrations are found in the Queyras metagabbros, a locality which is associated with open system interaction with sediment-derived fluids (Debret et al., 2016a), resulting in significant Fe isotope fractionation (Inglis et al., 2017).

A strong correlation is also found between $\delta^{60/58}$Ni and [Sb] (R^2=0.80) in the Queyras metagabbros (Fig. 3), consistent with enrichments found in serpentinites and transfer to the mantle wedge via subduction fluids (Deschamps et al., 2010). Antimony is thought to have similar incompatibility to Pr during MORB and OIB melt production (Jochum and Hofmann, 1997). In the samples studied here, the Sb/Pr is variable and higher in samples with lighter $\delta^{60/58}$Ni. Antimony is often carried in sediment-rich fluids and released from the slab in the early stages of subduction at <350 °C (Wu et al., 2021). Therefore, it makes sense that the highest Sb is observed in the blueschist samples at Queyras, which is the location with the greatest sediment-derived fluid contribution. In the metagabbros, lighter $\delta^{60/58}$Ni is also associated with higher concentrations of other fluid-mobile elements such as Ba (R^2 = 0.57), and Cs (R^2 = 0.36). Elemental ratios with Sb as well as Ba (as shown in Fig. 3) have previously been used to indicate fluid-rock interaction in these samples (Inglis et al., 2017). Note that the metasomatic effects in the blueschists cannot be related to retrograde fluids because this is a well-preserved prograde sequence without subsequent overprinting.

There is overwhelming evidence that Li, Rb, Sb, Cs and Ba are all highly mobile during sediment dehydration (e.g. Scambelluri et al., 2019). That these elements correlate with Ni isotopes in the Alpine blueschist metagabbros provides powerful evidence that fluid mobility is also responsible for this fractionation. In principle, this could be related to Ni either being added to, leached from, or exchanging with, the metagabbros. As stated above, the metagabbros have [Ni] that is not significantly lower than expected for their corresponding protoliths, providing no evidence for Ni addition or loss during metamorphism. The metasediments studied here have $\delta^{60/58}$Ni that is heavy; and the overwhelming majority of marine sediments also have heavy $\delta^{60/58}$Ni (e.g. Ciscato et al., 2018; He et al., 2023), although they are variable. There is no evidence that light $\delta^{60/58}$Ni has been added to the metagabbros from metasediment-derived fluids.

Recent studies have emphasized the role of ligand complexation in controlling stable isotope fractionation in high-pressure, high-temperature metasomatic environments (e.g. Debret et al., 2016b; Pons et al., 2016). It is therefore plausible that the Ni isotopic composition of the Queyras metagabbros reflects equilibrium with a fluid that preferentially complexes isotopically heavy Ni. Among the most isotopically heavy Ni complexes are aqueous sulfate ($Ni–SO_4(H_2O)_5$) and oxalate (NiC_2O_4) species (Fujii et al., 2011). Consequently, the formation of metamorphic minerals such as amphibole, mediated by the circulation of sulfate- or carbonate-rich fluids in an open system, would favour retention of isotopically light Ni in the solid phase and the release of isotopically heavy Ni in the fluid phase. Under this scenario, the Ni isotopic composition and concentration variability in metasomatized metagabbros likely reflect variations in fluid/rock ratios and fluid composition, which may explain the lack of correlation between these parameters.

Additional support for the mobility of Ni during subduction comes from arc volcanism. The nature of the fluids released during subduction-related phase transitions is redox-controlled and plays a key role in triggering melting of the mantle wedge and arc magmatism. Highly metasomatized peridotites, sampled as xenoliths from arc volcanoes, have been shown to contain more than ten times the Ni content of ambient mantle (Ishimaru and Arai, 2008), further supporting the idea that Ni is mobile in subduction and arc-related environments. Given that slab-derived fluids are known to be oxidizing (e.g. Debret and Sverjensky, 2017), we propose that such redox-driven processes control Ni isotope partitioning between the slab and metamorphic fluids at HP–HT conditions, thereby promoting the recycling of isotopically light Ni into the deep mantle.

The correlations between $\delta^{60/58}$Ni and concentrations of fluid-mobile elements such as Li and Sb in the eclogites and blueschists, are not found in present day MORB or OIB. Although this is consistent with loss of such elements from the slab to the overlying mantle wedge during subduction, as is well documented in arc systems, it leaves open the question of how Ni might have behaved. Note that the eclogitic metagabbros studied here, are not further metamorphosed equivalents of the blueschists, which were metasomatically altered by proximity to the Queyras metasediments. Therefore, they cannot be used as analogues of what would happen at greater depth with dehydration of the slab. Therefore, it currently is unclear if the fluids carrying Li and Sb from the slab would have also carried relatively heavy $\delta^{60/58}$Ni, as is predicted from the metamorphic fluid chemistry discussed above. This would have led to even lighter $\delta^{60/58}$Ni in the residual subducted slab. Further work is needed to verify whether, at the more extreme conditions of slab dehydration, this predicted relationship might break down.

6. Conclusions and implications for the Ni isotopic composition of the mantle

We have found evidence of Ni isotope fractionation accompanying high pressure metamorphism in subduction zone settings. The mafic assemblages studied have been affected by fluids carrying high concentrations of the fluid-mobile elements Li and Sb, demonstrating fluid infiltration associated with metamorphism. This is most pronounced for blueschist facies metamorphism. The concentrations of these elements correlate negatively with $\delta^{60/58}$Ni, probably caused by equilibrium isotopic fractionation between the metasomatic fluids and the residual Ni-depleted metamorphic assemblages.

Alternative explanations that light $\delta^{60/58}$Ni in metabasalts and metagabbros arises from alteration of the protoliths on the ocean floor are inconsistent with the extreme enrichment in fluid mobile elements, and the differing relations with chemical indices of magmatic enrichment recorded in MORB (Saunders et al. 2022). Furthermore, Ni isotopic fractionation associated with hydrothermal alteration of the oceanic crust is limited.

Abyssal peridotite $\delta^{60/58}$Ni is also presented here, but though very rich in Ni, is isotopically heavy – unlike the Alpine meta-igneous rocks studied, and also unlike all samples of MORB, OIB and peridotite xenoliths studied thus far. The $\delta^{60/58}$Ni forms a negative hyperbolic relationship with $^{187}Os/^{188}Os$, possibly implicating ancient fractionation of Ni isotopes and *Re*/Os, presumably related to sulfides in the mantle.

However, the possibility that this is related to alteration cannot be completely excluded. The origins of this fractionation warrant further study.

This study has presented clear evidence of fluid-mediated Ni isotope fractionation in subducting slabs, which over geological time could generate significant Ni isotopic variability in the asthenospheric mantle, consistent with the discovery of very light $\delta^{60/58}$Ni in pyroxenite xenoliths (Saunders et al., 2020). The signatures of Ni isotope fractionation correlating with concentrations of fluid-mobile elements such as Li and Sb in the eclogites and blueschists, are absent from present day MORB or OIB, consistent with loss of such elements from the slab to the overlying mantle wedge during subduction, as is well documented in arc systems. However, it is not yet clear whether the predicted transfer of heavy Ni based on metamorphic fluid chemistry will extend to all slab dehydration.

CRediT authorship contribution statement

Naomi J. Saunders: Writing – review & editing, Writing – original draft, Project administration, Methodology, Investigation, Formal analysis, Data curation. **Baptiste Debret:** Writing – review & editing, Resources. **Jason Harvey:** Writing – review & editing, Resources. **Edward Inglis:** Resources. **Alex N. Halliday:** Writing – review & editing, Supervision, Conceptualization.

Declaration of competing interest

The authors declare that they have no known competing financial interests or personal relationships that could have appeared to influence the work reported in this paper.

Acknowledgements

This work was supported by Columbia University. This research used samples provided by the Ocean Drilling Program (ODP), sponsored by the U.S. National Science Foundation and participating countries under the management of the Joint Oceanographic Institutions (JOI) Inc. We are grateful for helpful discussion with and comments from James Brennan, Kevin Burton, Rich Walker and Bernie Wood, as well as two anonymous reviewers.

Supplementary materials

Supplementary material associated with this article can be found, in the online version, at doi:10.1016/j.epsl.2025.119740.

Data availability

Data will be made available on request.

References

Agard, P., 2021. Subduction of oceanic lithosphere in the Alps: selective and archetypal from (slow-spreading) oceans. Earth-Sci. Rev. 214, 103517. https://doi.org/10.1016/j.earscirev.2021.103517.

Archer, C., Vance, D., Milne, A., Lohan, M.C., 2020. The oceanic biogeochemistry of nickel and its isotopes: new data from the South Atlantic and the Southern Ocean biogeochemical divide. Earth Planet. Sci. Lett. 535, 116118. https://doi.org/10.1016/j.epsl.2020.116118.

Bach, W., Garrido, C.J., Paulick, H., Harvey, J., Rosner, M., 2004. Seawater-peridotite interactions: first insights from ODP Leg 209, MAR 15°N. Geochem. Geophys. Geosystems 5. https://doi.org/10.1029/2004GC000744.

Cameron, V., Vance, D., 2014. Heavy nickel isotope compositions in rivers and the oceans. Geochim. Cosmochim. Acta 128, 195–211. https://doi.org/10.1016/j.gca.2013.12.007.

Caurant, C., Debret, B., Ménez, B., Nicollet, C., Bouilhol, P., 2023. Redox heterogeneities in a subducting slab: example from the Monviso meta-ophiolite (Western Alps, Italy). Lithos 446–447, 107136. https://doi.org/10.1016/j.lithos.2023.107136.

Chen, L.M., Lightfoot, P.C., Zhu, J.M., Teng, F.Z., Duan, Q., Yin, R., Wu, G., Yu, S.Y., Hu, R.Z., 2023. Nickel isotope ratios trace the process of sulfide-silicate liquid immiscibility during magmatic differentiation. Geochim. Cosmochim. Acta 353, 1–12. https://doi.org/10.1016/j.gca.2023.05.013.

Ciscato, E.R., Bontognali, T.R.R., Vance, D., 2018. Nickel and its isotopes in organic-rich sediments: implications for oceanic budgets and a potential record of ancient seawater. Earth Planet. Sci. Lett. 494, 239–250. https://doi.org/10.1016/j.epsl.2018.04.061.

Dale, C.W., Burton, K.W., Pearson, D.G., Gannoun, A., Alard, O., Argles, T.W., Parkinson, I.J., 2009. Highly siderophile element behaviour accompanying subduction of oceanic crust: whole rock and mineral-scale insights from a high-pressure terrain. Geochim. Cosmochim. Acta 73, 1394–1416. https://doi.org/10.1016/j.gca.2008.11.036.

Dale, C.W., Gannoun, A., Burton, K.W., Argles, T.W., Parkinson, I.J., 2007. Rhenium-osmium isotope and elemental behaviour during subduction of oceanic crust and the implications for mantle recycling. Earth Planet. Sci. Lett. 253, 211–225. https://doi.org/10.1016/j.epsl.2006.10.029.

Debret, Baptiste, Koga, K.T., Cattani, F., Nicollet, C., Van den Bleeken, G., Schwartz, S., 2016a. Volatile (Li, B, F and Cl) mobility during amphibole breakdown in subduction zones. Lithos 244, 165–181. https://doi.org/10.1016/j.lithos.2015.12.004.

Debret, B., Millet, M.A., Pons, M.L., Bouilhol, P., Inglis, E., Williams, H., 2016b. GSA Data Repository 2016064 isotopic evidence for iron mobility during subduction. Geology 44, 215–218. https://doi.org/10.1130/G37565.1.

Debret, B., Sverjensky, D.A., 2017. Highly oxidising fluids generated during serpentinite breakdown in subduction zones OPEN. Sci. Rep. 7, 1–6. https://doi.org/10.1038/s41598-017-09626-y.

Deschamps, F., Guillot, S., Godard, M., Chauvel, C., Andreani, M., Hattori, K., 2010. In situ characterization of serpentinites from forearc mantle wedges: timing of serpentinization and behavior of fluid-mobile elements in subduction zones. Chem. Geol. 269, 262–277. https://doi.org/10.1016/j.chemgeo.2009.10.002.

Dong, X.H., Wang, S.J., Pang, K.N., Shen, J., Chen, Y.X., Rostami-Hossouri, M., Ghasemi, H., 2024. The behavior of nickel isotopes during mantle melting. Geochim. Cosmochim. Acta 385, 34–44. https://doi.org/10.1016/j.gca.2024.10.002.

Elliott, T., Jeffcoate, A., Bouman, C., 2004. The terrestrial Li isotope cycle: light-weight constraints on mantle convection. Earth Planet. Sci. Lett. 220, 231–245. https://doi.org/10.1016/S0012-821X(04)00096-2.

Fan, Xuefei, Teng, Fang-Zhen, Berg, Anna D, Leeman, William, 2024. A global perspective on heavy Mg isotopic compositions of arc basalts. In: GOLDSCHMIDT - 2024 Goldschmidt Conference. Presented at the 2024 Goldschmidt Conference, Chicago.

Fleischmann, S., Du, J., Chatterjee, A., McManus, J., Iyer, S.D., Amonkar, A., Vance, D., 2023. The nickel output to abyssal pelagic manganese oxides: a balanced elemental and isotope budget for the oceans. Earth Planet. Sci. Lett. 619, 118301. https://doi.org/10.1016/j.epsl.2023.118301.

Fujii, T., Moynier, F., Dauphas, N., Abe, M., 2011. Theoretical and experimental investigation of nickel isotopic fractionation in species relevant to modern and ancient oceans. Geochim. Cosmochim. Acta 75, 469–482. https://doi.org/10.1016/j.gca.2010.11.003.

Gale, A., Dalton, C.A., Langmuir, C.H., Su, Y., Schilling, J.G., 2013. The mean composition of ocean ridge basalts. Geochem. Geophys. Geosyst. 14, 489–518. https://doi.org/10.1029/2012GC004334.

Gall, L., 2011. Development and application of nickel stable isotopes as a new geochemical tracer. University of Oxford.

Gall, L., Williams, H., Siebert, C., Halliday, A., 2012. Determination of mass-dependent variations in nickel isotope compositions using double spiking and MC-ICPMS. J. Anal. At. Spectrom. 27, 137–145. https://doi.org/10.1039/c1ja10209e.

Gall, L., Williams, H.M., Halliday, A.N., Kerr, A.C., 2017. Nickel isotopic composition of the mantle. Geochim. Cosmochim. Acta 199, 196–209. https://doi.org/10.1016/j.gca.2016.11.016.

Gall, L., Williams, H.M., Siebert, C., Halliday, A.N., Herrington, R.J., Hein, J.R., 2013. Nickel isotopic compositions of ferromanganese crusts and the constancy of deep ocean inputs and continental weathering effects over the Cenozoic. Earth Planet. Sci. Lett. 375, 148–155. https://doi.org/10.1016/j.epsl.2013.05.019.

Gannoun, A., Burton, K.W., 2014. High precision osmium elemental and isotope measurements of North Atlantic seawater. J. Anal Spectrom. 29, 2330–2342. https://doi.org/10.1039/C4JA00265B.

Godard, M., Awaji, S., Hansen, H., Hellebrand, E., Brunelli, D., Johnson, K., Yamasaki, T., Maeda, J., Abratis, M., Christie, D., Kato, Y., Mariet, C., Rosner, M., 2009. Geochemistry of a long in-situ section of intrusive slow-spread oceanic lithosphere: results from IODP Site U1309 (Atlantis Massif, 30°N Mid-Atlantic-Ridge). Earth Planet. Sci. Lett. 279, 110–122. https://doi.org/10.1016/j.epsl.2008.12.034.

Gueguen, B., Rouxel, O., 2021. The nickel isotope composition of the authigenic sink and the diagenetic flux in modern oceans. Chem. Geol. 563, 120050. https://doi.org/10.1016/j.chemgeo.2020.120050.

Gueguen, B., Rouxel, O., Fouquet, Y., 2021. Nickel isotopes and rare earth elements systematics in marine hydrogenetic and hydrothermal ferromanganese deposits. Chem. Geol. 560, 119999. https://doi.org/10.1016/j.chemgeo.2020.119999.

Gueguen, B., Rouxel, O., Ponzevera, E., Bekker, A., Fouquet, Y., 2013. Nickel isotope variations in terrestrial silicate rocks and geological reference materials measured by MC-ICP-MS. Geostand. Geoanalytic. Res. 37, 297–317. https://doi.org/10.1111/j.1751-908X.2013.00209.x.

Harvey, J., Gannoun, A., Burton, K.W., Rogers, N.W., Alard, O., Parkinson, I.J., 2006. Ancient melt extraction from the oceanic upper mantle revealed by re-Os isotopes in abyssal peridotites from the Mid-Atlantic ridge. Earth Planet. Sci. Lett. 244, 606–621. https://doi.org/10.1016/j.epsl.2006.02.031.

Hawco, N.J., Yang, S.C., Foreman, R.K., Funkey, C.P., Dugenne, M., White, A.E., Wilson, S.T., Kelly, R.L., Bian, X., Huang, K.F., Karl, D.M., John, S.G., 2020. Metal isotope signatures from lava-seawater interaction during the 2018 eruption of

Kīlauea. Geochim. Cosmochim. Acta 282, 340–356. https://doi.org/10.1016/j.gca.2020.05.005.
He, Z., Archer, C., Yang, S., Vance, D., 2023. Sedimentary cycling of zinc and nickel and their isotopes on an upwelling margin: implications for oceanic budgets and paleoenvironment proxies. Geochim. Cosmochim. Acta 343, 84–97. https://doi.org/10.1016/j.gca.2022.12.026.
Hofmann, A., Bekker, A., Dirks, P., Gueguen, B., Rumble, D., Rouxel, O.J., 2014. Comparing orthomagmatic and hydrothermal mineralization models for komatiite-hosted nickel deposits in Zimbabwe using multiple-sulfur, iron, and nickel isotope data. Miner. Deposita 49, 75–100. https://doi.org/10.1007/s00126-013-0476-1.
Inglis, E.C., Debret, B., Burton, K.W., Millet, M.A., Pons, M.L., Dale, C.W., Bouilhol, P., Cooper, M., Nowell, G.M., McCoy-West, A.J., Williams, H.M., 2017. The behavior of iron and zinc stable isotopes accompanying the subduction of mafic oceanic crust: a case study from Western Alpine ophiolites. Geochem. Geophys. Geosyst. 18, 1711–1738. https://doi.org/10.1002/2016GC006735.Received.
Ishimaru, S., Arai, S., 2008. Nickel enrichment in mantle olivine beneath a volcanic front. Contrib. Mineral. Petrol. 156, 119–131. https://doi.org/10.1007/s00410-007-0277-6.
Jochum, K.P., Hofmann, A.W., 1997. Constraints on earth evolution from antimony in mantle-derived rocks. Chem. Geol. 139, 39–49. https://doi.org/10.1016/S0009-2541(97)00032-6.
Kelemen, P.B., Kikawa, E., Meller, D.J., .2004. Site 1274, Proceedings of the Ocean Drilling Program, Initial Reports volume 209.
Kelemen, Peter.B., E, K., Miller, D.J., 2004. Site 1268, Proceedings of the Ocean Drilling Program, Initial Reports volume 209.
Klaver, M., Elliott, T., Ionov, D.A., Bizimis, M., Berndt, J., Klemme, S., 2024. Nickel isotope fractionation factors between silicate minerals and melt. Geochim. Cosmochim. Acta 366, 221–236. https://doi.org/10.1016/j.gca.2023.11.026.
Klaver, M., Ionov, D.A., Takazawa, E., Elliott, T., 2020. The non-chondritic Ni isotope composition of Earth's mantle. Geochim. Cosmochim. Acta 268, 405–421. https://doi.org/10.1016/j.gca.2019.10.017.
Klein, F., Bach, W., 2009. Fe-Ni-Co-O-S phase relations in peridotite-seawater interactions. J. Petrol. 50, 37–59. https://doi.org/10.1093/petrology/egn071.
Lemaitre, N., Du, J., de Souza, G.F., Archer, C., Vance, D., 2022. The essential bioactive role of nickel in the oceans: evidence from nickel isotopes. Earth Planet. Sci. Lett. 584, 117513. https://doi.org/10.1016/j.epsl.2022.117513.
Little, S.H., Archer, C., McManus, J., Najorka, J., Wegorzewski, A.V., Vance, D., 2020. Towards balancing the oceanic Ni budget. Earth Planet. Sci. Lett. 547, 116461. https://doi.org/10.1016/J.EPSL.2020.116461.
Machado, A.L., Garnier, J., Ratié, G., Guimaraes, E., Monvoisin, G., Cloquet, C., Quantin, C., 2023. Nickel mass balance and isotopic records in a serpentinic weathering profile: implications on the continental Ni budget. Chem. Geol. 634, 121586. https://doi.org/10.1016/j.chemgeo.2023.121586.
McDonough, W.F., Sun, S.s., 1995. The composition of the Earth. Chem. Geol. 120, 223–253. https://doi.org/10.1016/0009-2541(94)00140-4.
Miller, D.J., 2007. Sulfide mineralization AT site 1268, mid-atlantic ridge, ocean drilling program leg 2091. In: Kelemen, P.B., Kikawa, E., Miller, D.J. (Eds.), Proceedings of the Ocean Drilling Program, 209 Scientific Results, Proceedings of the Ocean Drilling Program. Ocean Drilling Program. https://doi.org/10.2973/odp.proc.sr.209.2007.
Palme, H., O'Neill, H.St.C.S.C., 2007. Cosmochemical estimates of mantle composition. Treatise Geochem. 1–38. https://doi.org/10.1016/B0-08-043751-6/02177-0.
Pašava, J., Chrastný, V., Loukola-Ruskeeniemi, K., Šebek, O., 2019. Nickel isotopic variation in black shales from Bohemia, China, Canada, and Finland: a reconnaissance study. Miner. Deposita 54, 719–742. https://doi.org/10.1007/s00126-018-0839-8.
Paulick, H., Bach, W., Godard, M., De Hoog, J.C.M., Suhr, G., Harvey, J., 2006. Geochemistry of abyssal peridotites (Mid-Atlantic Ridge, 15°20′N, ODP Leg 209): implications for fluid/rock interaction in slow spreading environments. Chem. Geol. 234, 179–210. https://doi.org/10.1016/j.chemgeo.2006.04.011.
Pons, M.L., Debret, B., Bouilhol, P., Delacour, A., Williams, H., 2016. Zinc isotope evidence for sulfate-rich fluid transfer across subduction zones. Nat. Commun. 7, 1–8. https://doi.org/10.1038/ncomms13794.
Porter, S.J., Selby, D., Cameron, V., 2014. Characterising the nickel isotopic composition of organic-rich marine sediments. Chem. Geol. 387, 12–21. https://doi.org/10.1016/j.chemgeo.2014.07.017.
Ratié, G., Jouvin, D., Garnier, J., Rouxel, O., Miska, S., Guimarães, E., Cruz Vieira, L., Sivry, Y., Zelano, I., Montarges-Pelletier, E., Thil, F., Quantin, C., 2015. Nickel isotope fractionation during tropical weathering of ultramafic rocks. Chem. Geol. 402, 68–76. https://doi.org/10.1016/j.chemgeo.2015.02.039.
Ratié, G., Quantin, C., Jouvin, D., Calmels, D., Ettler, V., Sivry, Y., Vieira, L.C., Ponzevera, E., Garnier, J., 2016. Nickel isotope fractionation during laterite Ni ore smelting and refining: implications for tracing the sources of Ni in smelter-affected soils. Appl. Geochem. 64, 136–145. https://doi.org/10.1016/j.apgeochem.2015.09.005.
Ravizza, G., Norris, R.N., Blusztajn, J., Aubry, M.P., 2001. An osmium isotope excursion associated with the late paleocene thermal maximum: evidence of intensified chemical weathering. Paleoceanography 16, 155–163. https://doi.org/10.1029/2000PA000541.
Saunders, N.J., Barling, J., Harvey, J., Fitton, J.G., Halliday, A.N., 2022. Heterogeneous nickel isotope compositions of the terrestrial mantle – Part 2: mafic lithologies. Geochim. Cosmochim. Acta 317, 349–364. https://doi.org/10.1016/J.GCA.2021.11.011.
Saunders, N.J., Barling, J., Harvey, J., Halliday, A.N., 2020. Heterogeneous nickel isotopic compositions in the terrestrial mantle – Part 1: ultramafic lithologies. Geochim. Cosmochim. Acta 285, 129–149. https://doi.org/10.1016/j.gca.2020.06.029.
Scambelluri, M., Cannaò, E., Gilio, M., 2019. The water and fluid-mobile element cycles during serpentinite subduction. A review. Eur. J. Mineral. 31, 405–428. https://doi.org/10.1127/ejm/2019/0031-2842.
Scambelluri, M., Philippot, P., 2001. Deep fluids in subduction zones. Lithos, Fluid inclusions: phase relationships - methods - applications. A special issue in honour of Jacques Touret 55, 213–227. https://doi.org/10.1016/S0024-4937(00)00046-3.
Schwartz, S., Guillot, S., Reynard, B., Lafay, R., Debret, B., Nicollet, C., Lanari, P., Auzende, A.L., 2013. Pressure–temperature estimates of the lizardite/antigorite transition in high pressure serpentinites. Lithos, Serpentinites from mid-oceanic ridges to subduction 178, 197–210. https://doi.org/10.1016/j.lithos.2012.11.023.
Sheng, S.Z., Wang, S.J., Yang, X.M., Chen, L.H., Zeng, G., Xiao, Y., Shen, J., Dong, X.H., Lv, Y.W., 2022. Sulfide dissolution on the nickel isotopic composition of basaltic rocks. J. Geophys. Res. Solid Earth 127, e2022JB024555. https://doi.org/10.1029/2022JB024555.
Smith, J.M., Ripley, E.M., Li, C., Wasylenki, L.E., 2022. Cu and Ni Isotope Variations of Country Rock-Hosted Massive Sulfides Located Near Midcontinent Rift Intrusions. Econ. Geol. 117 (1), 195–211. https://doi.org/10.5382/econgeo.4872.
Spivak-Birndorf, L.J., Wang, S.J., Bish, D.L., Wasylenki, L.E., 2018. Nickel isotope fractionation during continental weathering. Chem. Geol. 476, 316–326. https://doi.org/10.1016/J.CHEMGEO.2017.11.028.
Sun, S.S., Deng, T.H.B., Ao, M., Yang, W.J., Liu, X.R., Liu, T., Zhu, J.M., Morel, J.L., Tang, Y.T., Qiu, R.L., 2024. Nickel isotope fractionation during intense weathering of basalt: implications for Ni output from continental weathering. Geochim. Cosmochim. Acta 367, 107–122. https://doi.org/10.1016/j.gca.2023.12.023.
Takano, S., Liao, W.H., Ho, T.Y., Sohrin, Y., 2022. Isotopic evolution of dissolved Ni, Cu, and Zn along the Kuroshio through the East China Sea. Mar. Chem. 243. https://doi.org/10.1016/J.MARCHEM.2022.104135.
Takano, S., Tanimizu, M., Hirata, T., Shin, K.C., Fukami, Y., Suzuki, K., Sohrin, Y., 2017. A simple and rapid method for isotopic analysis of nickel, copper, and zinc in seawater using chelating extraction and anion exchange. Anal. Chim. Acta 967, 1–11. https://doi.org/10.1016/j.aca.2017.03.010.
Tricart, P., Schwartz, S., 2006. A north-south section across the Queyras Schistes lustrés (Piedmont zone, Western Alps): syn-collision refolding of a subduction wedge. Eclogae Geol. Helvetiae. 99, 429–442. https://doi.org/10.1007/s00015-006-1197-6.
Wang, R.M., Archer, C., Bowie, A.R., Vance, D., 2019. Zinc and nickel isotopes in seawater from the Indian Sector of the Southern Ocean: the impact of natural iron fertilization versus Southern Ocean hydrography and biogeochemistry. Chem. Geol. 511, 452–464. https://doi.org/10.1016/J.CHEMGEO.2018.09.010.
Wang, S.J., Wang, W., Zhu, J.M., Wu, Z., Liu, J., Han, G., Teng, F.Z., Huang, S., Wu, H., Wang, Y., Wu, G., Li, W., 2021. Nickel isotopic evidence for late-stage accretion of Mercury-like differentiated planetary embryos. Nat. Commun. 12, 1–7. https://doi.org/10.1038/s41467-020-20525-1.
Wu, G., Zhu, J.M., Wang, X., Johnson, T.M., He, Y., Huang, F., Wang, L.X., Lai, S.C., 2022. Nickel isotopic composition of the upper continental crust. Geochim. Cosmochim. Acta 332, 263–284. https://doi.org/10.1016/j.gca.2022.06.019.
Wu, K., Zhang, L., Yuan, H., Sun, W., Deng, J., Zartman, R.E., Guo, J., Bao, Z., Zong, C., 2021. Boron, arsenic and antimony recycling in subduction zones: new insights from interactions between forearc serpentinites and CO2-rich fluids at the slab-mantle interface. Geochim. Cosmochim. Acta 298, 21–42. https://doi.org/10.1016/j.gca.2021.01.039.
Yang, X., Wang, S., Zhang, Y., Dong, X., Teng, F., Helz, R.T., Huang, J., Li, X., Huang, S., 2023. Nickel isotope fractionation during magmatic differentiation. Geochem. Geophys. Geosyst. 24, e2023GC010926. https://doi.org/10.1029/2023GC010926.
Yuan, S., Li, H., Arculus, R.J., He, Y., Ke, S., Sun, W., 2023. Heavy magnesium isotopic compositions of basalts erupted during arc inception: implications for the mantle source underlying the nascent Izu-Bonin-Mariana arc. Geochim. Cosmochim. Acta 352, 14–23. https://doi.org/10.1016/j.gca.2023.04.017.
Zhang, Y., Yuan, C., Sun, M., Chen, M., Hong, L., Li, J., Long, X., Li, P., Lin, Z., 2019. Recycled oceanic crust in the form of pyroxenite contributing to the cenozoic continental basalts in central Asia: new perspectives from olivine chemistry and whole-rock B–Mo isotopes. Contrib. Mineral. Petrol. 174, 83. https://doi.org/10.1007/s00410-019-1620-4.